Radiation Characteristics of Differentially-Fed Dual Circularly Polarized GNSS Antenna

M. Berg[1], J. Chen[1], A. Pärssinen[1],
[1]Centre for Wireless Communications - Radio Technologies Research Unit (CWC-RT), University of Oulu, Finland,
markus.berg@oulu.fi

***Abstract*—This paper discusses the method to create a dual circular polarized antenna for GNSS applications. First time, the differentially-driven circular patch is demonstrated to create a feasible cross-polarization discrimination (XPD) for phase accurate antenna structure. Traditional choke rings are applied to control the radiation pattern characteristics. A separate feed network is used to obtain simultaneous left and right hand circular polarizations for the corresponding coaxial connectors of the antenna. The operation of the feed network is described by using a block diagram. Resulting antenna radiation parameters include max. gain of 6.2 dB, axial ratio $<$ 3 dB over the upper hemisphere for the frequency range 1.55-1.61 GHz. The simulated antenna response for right hand polarized plane wave excitation demonstrate 27-29 dB isolation between the left and right hand antenna ports.**

***Index Terms*—circular patch, differential feed, dual polarized, GNSS.**

I. Introduction

The commercial Global Navigation Satellite Systems (GNSS) - including GPS, GLONASS and GALILEO - have been widely deployed for military and commercial use. The geographically limited satellite navigation systems are emerging and include Chinese BeiDou, Indian Navic, and Japanese Quasi-Zenith Satellite System (QZSS). Because of the benefits of global positioning, emerging application areas such as autonomous vessels and robot cars are typically equipped with GNSS positioning in addition to short-range sensing and localization systems.

The accuracy of the satellite positioning can be improved by using the Real Time Kinematic (RTK) measurement method, in which the carrier phase measurement and the use of at least one on-ground reference station are utilized [1]. This is currently a conventional positioning method in geodesy and excavation. However, RTK requires phase calibrated antennas and for the increased positioning accuracy also dual-band receivers.

Current state-of-the-art antenna solutions for geodetic applications include mainly single circularly polarized (CP) receiving antennas for multi- or dual-band use, such as [2]. This is understandable because of the fundament of GNSS. Also, the commercial receivers support the use of single polarized antennas only. However, there is a clear evidence that in addition to the reception of the right hand circular polarized (RC) wave, which is the specified system polarization, the simultaneous reception of the left hand circular polarized (LC) wave enable the wave propagation environment sensing [3], or more robust positioning for partially depolarized GNSS signals [4], [5]. The wave depolarization can be due to the multipath and/or shadow propagation environment.

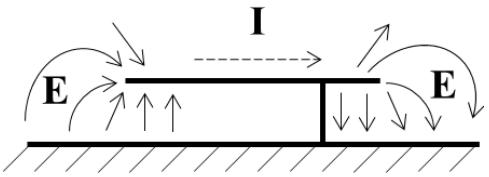

Fig. 1. Illustration of the electric field **E** and current **I** distributions for the on-ground patch antenna

Potential applications of this dual polarized GNSS method include e.g. autonomous driving and vegetation sensing, which would benefit from the additional information of the positioning inaccuracy. The dual polarized receiver approach require GNSS receiving antennas including dual circular polarization, low cross polarization discrimination (XPD) for both polarizations, equal phase centers for both LC and RC polarizations, and stable phase radiation patterns. So far, only few dual-circularly polarized antennas have been proposed for the emerging GNSS based environmental sensing [6].

In this paper, we examine the feasibility and the performance of the differential antenna feed concept to obtain the mentioned antenna requirements for a dual circularly polarized GNSS receiving antenna.

II. Differential Antenna Feed

In electromagnetics, the term differential can be understood to mean the electric current **I** or electric field **E** having equal amplitude but opposite direction. By considering the electric field distribution of the patch antenna, as shown in Fig. 1, it is observed that the fundamental radiation mode is based on the differential field distribution. By mirroring the feed to the opposite side in regard to patch centre yield to opposite excitation current. Thus, the differential antenna feed comprises two spatially separated symmterical feeds exciting the same polarization of the antenna with opposite excitation phases [7]. The operation principle of the differentially-driven microstrip antenna can be explained e.g. by the cavity model [8].

The advantage of the differential feed include low cross polarization discrimination (XPD) level. The differential feed

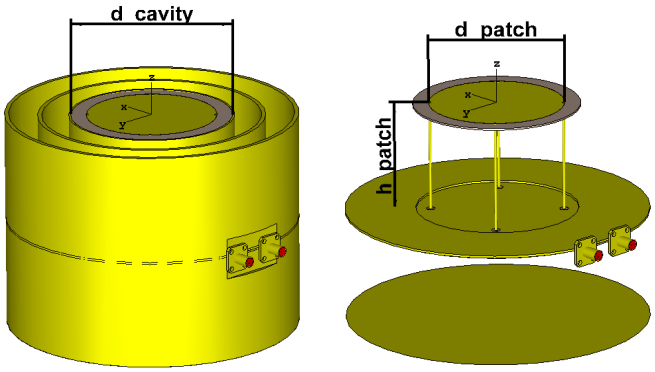

Fig. 2. Dual circularly polarized GNSS antenna (left), and the internal patch structure when the cavity and choke rings are hidden (right)

solutions have been examined for e.g. single-polarized antenna arrays requiring controlled radiation pattern over wide bandwidth [9], and dual-linearly polarized subarrays for satellite synthetic aperture radar [10].

A common and simple feeding method of the patch is a direct coaxial-type of feed. The patch input impedance is a function of the feed distance from the center of the antenna. A feed inset is typically used to match the patch antenna impedance to the characteristic $50\ \Omega$ of the waveguide. However, the antenna form factor can be optimized so that it yield advantageous impedance in the outer edges of the patch, or if discrete matching components are used, then the feed location of the antenna can be selected quite freely. The former method is used in this GNSS antenna examination.

III. Antenna Structure

The antenna examined in this paper is a circular patch antenna ($d_{patch} = 63$ mm) having two orthogonal differential feed pairs (depicted in Fig. 2). The patch substrate is FR-4 with thickness of 0.8 mm and the antenna height from the ground is 52 mm. Rotational symmetry is exploited for circular polarization. The patch is surrounded by a cavity with diameter of $d_{cavity} = 76$ mm to generate adequate input impedance for the differential feeds. Two antenna centric choke rings are used to decrease the gain in the horizontal plane and to increase the front-to-back (F/B) ratio of the antenna. For antenna design and simulation, a full wave 3D simulation software CST Studio Suite is used.

The dual polarized antenna feed arrangement consists of two antenna connectors (one for each polarization), a miniaturized branch-line coupler with 90° phase difference between two outputs, two Wilkinson power dividers [11], and the phase-optimized microstrip feed lines for the vertical antenna feeds. The block diagram of the feed network is illustrated in Fig. 3 together with the relative phases in each stage for RC polarization. The operation of the feed arrangement is described here from the transmission perspective for straightforward understanding, but in case of the GNSS signal reception the operation is reverse. The four-port branch-line coupler

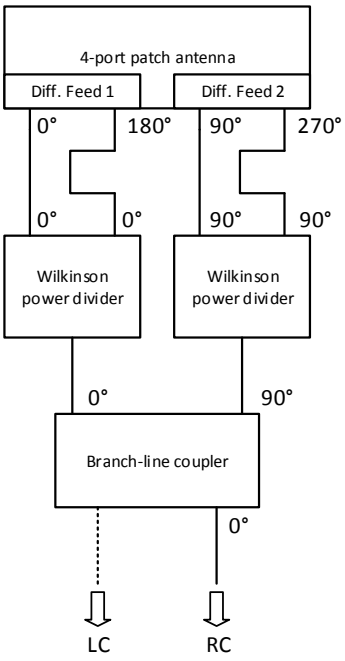

Fig. 3. Block diagram of the differential feed arrangement

is used to obtain the required 90° phase difference for the orthogonal antenna feeds required for simultaneous LC and RC polarizations. The coupler is optimized for 1.575 GHz and miniaturized by meandering the striplines. Miniaturization has a minor effect on the isolation between connector ports, but enables increased distance to other feed structure near the interconnection from the microstrip to the vertical feed. Both outputs of the coupler are split to two by Wilkinson power divider in order to generate equal power levels for the differential antenna feeds. Feed network is enclosed by a cylinder and a related bottom end, both made of brass (also illustrated in Fig. 2).

IV. Simulation and Measurement Results

The prototype antenna has been fabricated. The cylindrical cavity and choke rings have been made of brass with thickness of 0.2 mm. Antenna patch and microstrip lines have been etched to the standard FR-4 PCB. Authors have a strong comprehension that the simulation results will match to the measured performance, because of their prior work in the antenna design of the same type [6], [12].

The operation principle of the differential antenna excitation is illustrated in Fig. 4 by simulated E-field magnitude. Two orthogonal resonance modes of the antenna are excited with a phase difference of 90° to obtain the RC polarization. Simultaneously, the feed network realizes an opposite phase difference for the LC polarization.

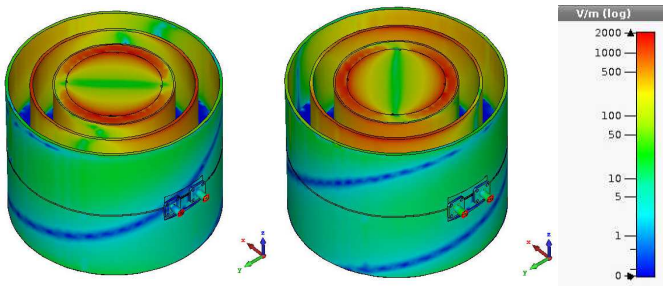

Fig. 4. Simulated E-field magnitudes for the orthogonal resonance modes of the antenna at 1.575 GHz. Field plots of the phases 0° and 90° are shown for the RC polarized wave

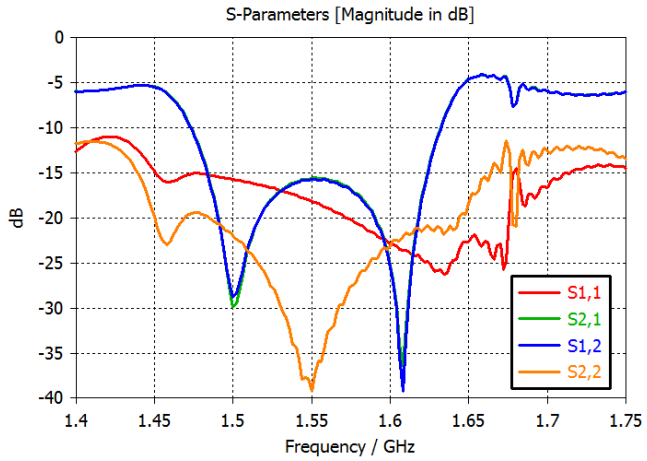

Fig. 5. Simulated scattering parameters S_{11} and S_{22} indicate good impedance matching. Isolation between LC and RC ports (S_{12}, S_{21}) is moderate.

A. S-parameters

The simulated impedance matching to coaxial 50 Ω feed connectors over the L1, G1 and E1 bands are shown by S_{11} and S_{22} parameters in Fig. 5 for both LC and RC ports together with the port isolations. Difference between the input reflection coefficients are due to the asymmetric feed network required for the 90° phase difference between the differential feed pairs. Port isolation (S_{21} and S_{12}) is > 15 dB over the band, which can be considered as tolerable for reception antennas. Main reason for the moderate isolation is the cross coupling in the microstrip feed network enclosed in the metal cavity.

B. Gain and Axial Ratio

Gain patterns are optimized to cover efficiently the upper hemisphere and the choke rings are used to suppress the horizontal gain and to increase the F/B ratio. The simulated co-polar and cross-polar gains for RC are shown in Fig. 6. The co-polar realized gain varies from -8 dB to 6.2 dB over the targeted elevation angles $-90° \leq \theta \leq 90°$. Cross-polarization levels are ≤ -20 dB and ≤ -25 dB for 1.55 GHz and 1.61 GHz, respectively. The corresponding LC radiation patterns are identical to the RC patterns.

The simulated axial ratios (AR) for both LC an RC ports are depicted in Fig. 7 as a function of θ and ϕ. For the intended

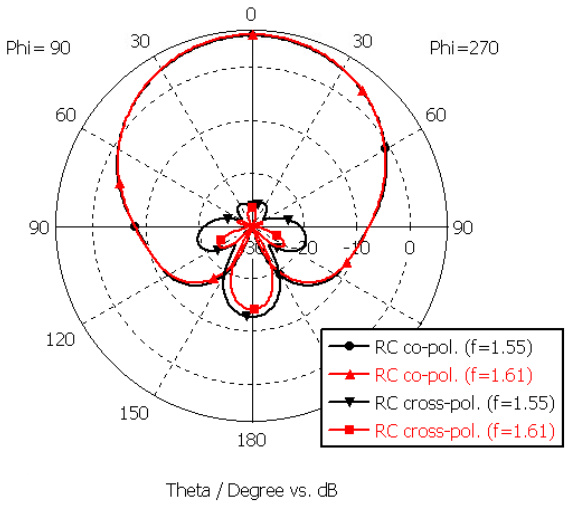

Fig. 6. Co- and cross-polar radiation patterns for RC at 1.55 GHz and 1.61 GHz ($\phi = 90°$).

angular domain, the simulated AR is ≤ 2 dB at 1.61 GHz. For the lower band edge at 1.55 GHz, the corresponding AR is ≤ 3 dB. This is the typical level of the single circular polarized geodetic GNSS antennas [2], but achieved now simultaneously with the dual circular polarized antenna. The effect of the rotational symmetry of the antenna structure result to stable azimuthal plane behaviour, whereas the low AR in the elevation plane ($\theta \leq 90°$) is due to the differential feed.

C. Phase pattern

For the geodetic GNSS antennas, the phase response is important because of the measurement method which utilize the carrier phase measurement to improve the positioning accuracy. Targeted phase pattern variation of the geodetic antennas is as small as possible, being only few degrees. The phase pattern can be measured and the data used for the phase calibration in the receiver, but the smaller variation reduces the potential angle error arising from the inaccurate antenna positioning during the measurement. The simulated phase response for both LC and RC ports of the antenna are illustrated in Fig. 8 as a function of the elevation angle for $\phi = 0°$ and $\phi = 90°$. The maximum phase difference over the targeted angular range is $\leq 10°$.

D. Simulated RC Plane Wave Reception

The reception properties of the antenna were simulated by modelling RC plane wave excitation from the boresight direction. Waveguide ports were used in the coaxial LC and RC connectors to compare their mutual field strengths. Simulation results are shown in Fig. 9, clearly indicating 27...29 dB difference in the received field strength over the targeted frequency band $1.55 - 1.61$ GHz. The moderate port isolation shown in Fig. 5 in case of the transmission is not a major problem in the reception. This is because of the directional properties of the hybrid coupler. The receiving performance of the antenna means that in practical GNSS field

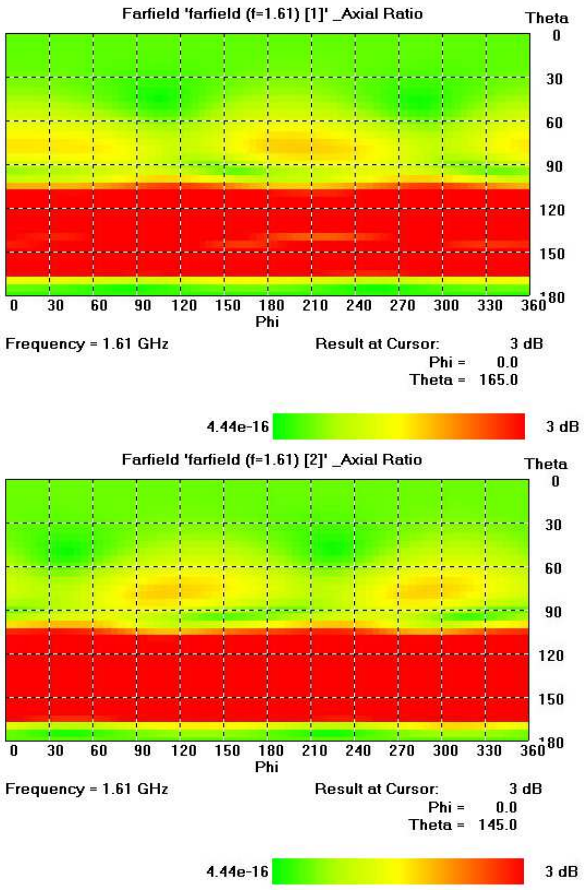

Fig. 7. Simulated axial ratios for RC (top) and LC (bottom) at 1.61 GHz.

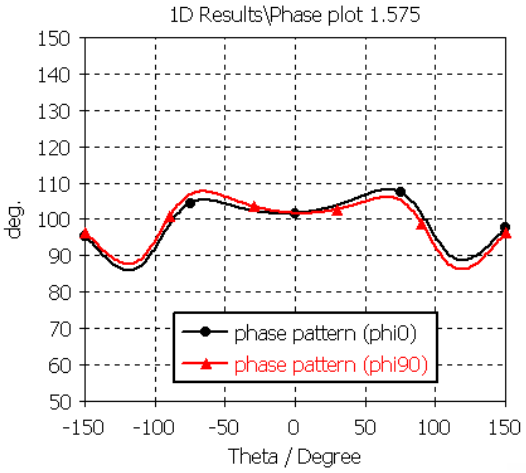

Fig. 8. Simulated RC phase pattern at 1.61 GHz.

measurements, the achievable resolution between LC and RC ports is feasible to separate the right- and left-hand polarized direct or multipath propagation components.

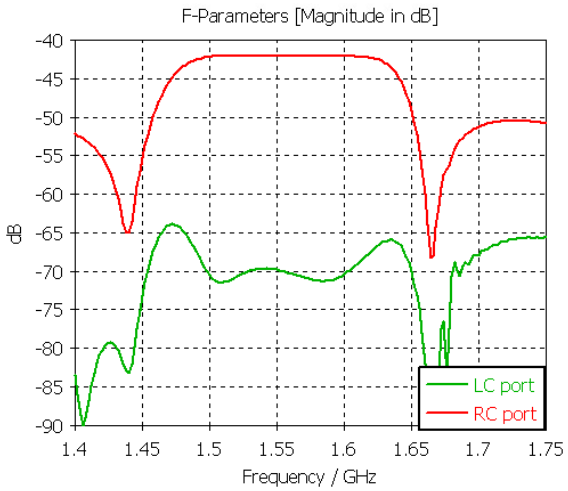

Fig. 9. Simulated F-parameters show the receiver LC and RC port field strengths relative to the RC plane wave excitation.

V. Conclusion

A dual circularly polarized GNSS reception antenna for the high accurate positioning and the multipath propagated signal evaluation is proposed. Antenna comprises the differentially-driven circular patch with orthogonal feeds for circular polarizations. Separate feed network is used to create simultaneous LC and RC polarizations accessed through separate coaxial connectors. Antenna has gain of 6.2 dB and AR $\leq$ 3 dB over the targeted elevation angles $-90° \leq \theta \leq 90°$. These performance figures are achieved simultaneously for LC and RC polarizations by single antenna. Further, the phase pattern variation of the beam is $< 10°$. This antenna structure enable further increased accuracy for the positioning and the propagation environment sensing.

Acknowledgment

This work was supported in part by the Academy of Finland 6Genesis Flagship (grant no. 318927).

References

[1] N. C. Talbot, "Centimeters in the Field, a Users Perspective of Real-time Kinematic Positioning in a Production Environment," Proceedings of the 6th International Technical Meeting of the Satellite Division of The Institute of Navigation (ION GPS 1993), Salt Lake City, UT, September 1993, pp. 1049-1057.

[2] S. Liu, D. Li, B. Li and F. Wang, "A Compact High-Precision GNSS Antenna With a Miniaturized Choke Ring," in IEEE Antennas and Wireless Propagation Letters, vol. 16, pp. 2465-2468, 2017. doi: 10.1109/LAWP.2017.2724302

[3] R. U. R. Lighari, E. T. Salonen, M. Berg, and A. Pärssinen. Analysis of GPS Reected Signals Based on SNR Measurements: Land Versus Water. In Proc. 12th European Conference on Antennas and Propagation (EuCAP 2018), London, UK, April 9-13, 2018. doi: 10.1109/LAPC.2016.7807561

[4] M. Ibraheam et al., "Feasibility of dual-polarized antenna arrays for GNSS receivers at low elevations," 2017 11th European Conference on Antennas and Propagation (EUCAP), Paris, 2017, pp. 857-861. doi: 10.23919/EuCAP.2017.7928441

[5] N. Capet, and F-X. Marmet, "Multipath mitigation in a GNSS radio receiver," US Patent 2018/0180742 A1, Jun 28, 2018

[6] M. Berg, R. U. R. Lighari, T. Tuovinen and E. T. Salonen, "Circularly polarized GPS antenna for simultaneous LHCP and RHCP reception with high isolation," 2016 Loughborough Antennas and Propagation Conference (LAPC), Loughborough, 2016, pp. 1-4.

[7] T. Brauner, R. Vogt and W. Bachtold, "A differential active patch antenna element for array applications," in IEEE Microwave and Wireless Components Letters, vol. 13, no. 4, pp. 161-163, April 2003. doi: 10.1109/LMWC.2003.811045

[8] Y. P. Zhang and J. J. Wang, "Theory and analysis of differentially-driven microstrip antennas," in IEEE Transactions on Antennas and Propagation, vol. 54, no. 4, pp. 1092-1099, April 2006. doi: 10.1109/TAP.2006.872597

[9] H. Jin, K. Chin, W. Che, C. Chang, H. Li and Q. Xue, "Differential-Fed Patch Antenna Arrays With Low Cross Polarization and Wide Bandwidths," in IEEE Antennas and Wireless Propagation Letters, vol. 13, pp. 1069-1072, 2014. doi: 10.1109/LAWP.2014.2328352

[10] X. Zhao, B. N. Tian, S. P. Yeo and L. C. Ong, "Low-Profile Broadband Dual-Polarized Integrated Patch Subarray for X-Band Synthetic Aperture Radar Payload on Small Satellite," in IEEE Antennas and Wireless Propagation Letters, vol. 16, pp. 1735-1738, 2017.

[11] E. J. Wilkinson, "An N-Way Hybrid Power Divider," in IRE Transactions on Microwave Theory and Techniques, vol. 8, no. 1, pp. 116-118, January 1960. doi: 10.1109/TMTT.1960.1124668

[12] R. U. R. Lighari, E. T. Salonen, M. Berg, and A. Pärssinen. Analysis of GPS Reected Signals Based on SNR Measurements: Land Versus Water. In Proc. 12th European Conference on Antennas and Propagation (EuCAP 2018), London, UK, April 9-13, 2018.